The Sensitivity of Aerodynamic Forces to Multi-parameters in a Bird-like Flapping Wing

Changtao Ding*, Yuanjun Lv & Min Lu

Zhejiang Industry Polytechnic College, No.151 Qutun Road, Shaoxing 312000, China
*E-mail: ctding@zju.edu.cn

Abstract. The sensitivity of aerodynamic forces in a bird-like flapping wing was numerically studied by analyzing the aerodynamic force states under different parameters. First, the physical model and the kinematic model of the bird-like flapping wing were separately established. Then the aerodynamic force model was established and some important parameters were analyzed by adopting the Taguchi orthogonal method. Finally, a simulation was carried out, from which the order of the parameters was separately determined according to the parameters' effect on lift or thrust. The results showed that increasing the flapping frequency is one of the most important ways to increase lift and thrust. The lift can be increased by increasing the flight velocity, while the thrust can be increased by increasing the maximum flapping angle. The lift or the thrust becomes larger when the incidence angle is approximately $35°$ or $55°$.

Keywords: *aerodynamic forces; bird-like flapping wing; flapping frequency; multi-parameters; Taguchi orthogonal method.*

1 Introduction

The aerodynamic forces of a bird-like flapping wing mainly consist of lift and thrust. The values of these forces directly determine the flying state of a flapping wing robot. When the values are large enough, the robot can carry a heavy weight to complete some tasks, such as carrying cameras to capture bird habits. The aerodynamic forces are determined by several parameters [1]. Therefore, it is important to study which parameters affect the aerodynamic forces with the aim of realizing the robot flight.

Many researchers have widely studied the aerodynamic forces of bird-like flapping wings in recent decades. Stewart, *et al.* adopted both Peters' aerodynamics and the blade element theory to calculate the aerodynamic forces of a flapping wing [2]. In [3], the force of a flapping wing under hovering condition was investigated based on the unsteady blade element theory. Using an unsteady aerodynamic model, Sujoy, *et al.* obtained the aerodynamic forces of a flapping wing actuated by a lead zirconate titanate (PZT) unimorph [4]. In [5], an unsteady blade element theory model was presented to calculate the aerodynamic forces and the inertial force of a 3D flapping wing. Yang, *et al.*

Received April 9th, 2018, Revised August 23rd, 2018, Accepted for publication November 1st, 2018.
 ISSN: 2337-5779, DOI: 10.5614/j.eng.technol.sci.2018.50.5.5

analyzed the aerodynamic forces of a flapping wing robot by solving the Navier-Stokes equations (N-S equations) in the Fluent software [6]. The temporal and spatial aerodynamic forces of a flexible flapping wing were separately obtained based on the Digital Image Correlation and the Computational Fluid Dynamics (CFD) method in [7]. According to the computed and measured force data, Vinh adopted the panel method and the Fluent software to solve the aerodynamic force of a flapping wing at a low Reynolds number in [8]. Zhang, *et al.* solved the aerodynamic force of a flapping wing with the unsteady vortex lattice method in [9].

Several researchers have studied the parameter influences on the performance of a flapping wing robot. The aerodynamic performance of a flapping wing was investigated by solving the N-S equations and the results indicate that the wingspan's flexible deformation should be limited to enhance the aerodynamic performance [10]. The results in [11] indicate that the wing-wake interaction can result in both lift enhancement and reduction. The aerodynamic performance of a butterfly wing was studied under different parameters such as the Reynolds number, the advance ratios and the flapping frequency in [12]. Zhu, *et al.* established the incompressible N-S equations to investigate the aerodynamic performance of a flapping wing and the results indicate that the aerodynamic characteristics of a wing can be affected by its geometry [13]. To the best of our knowledge, we identify for the first time that minimal attention has been paid to the sensitivity of aerodynamic forces to multi-parameters. However, single or multiple parameters have a great impact on aerodynamic forces, which is significant for further studies.

Based on the physical model, the kinematic model and the aerodynamic model of a flapping wing, the sensitivity of aerodynamic forces was studied under different parameters. This paper is organized as follows: the physical model and the kinematic model of a bird-like flapping wing are established in Section 2. In Section 3, the flapping wing aerodynamic model is established. In addition, the influences of the parameters and their combinations are analyzed using the Taguchi orthogonal method. The numerical analysis and the conclusion are respectively described in Sections 4 and 5. Additionally, this study provides a theoretical basis for adjusting the aerodynamic forces of a bird-like flapping wing robot.

2 The Kinematic Model of a Bird-like Flapping Wing

Flapping wings have a super-strong ability to adjust aerodynamic forces. Figures 1(a)-(f) are respectively the flapping wing photographs of the golden eagle, the barn owl, the red-crowned crane, the sea eagle, the bald eagle, and the

black-footed albatross [14-19]. The common features of the abovementioned flapping wings are that they are wide and approximate the shape of a rectangle.

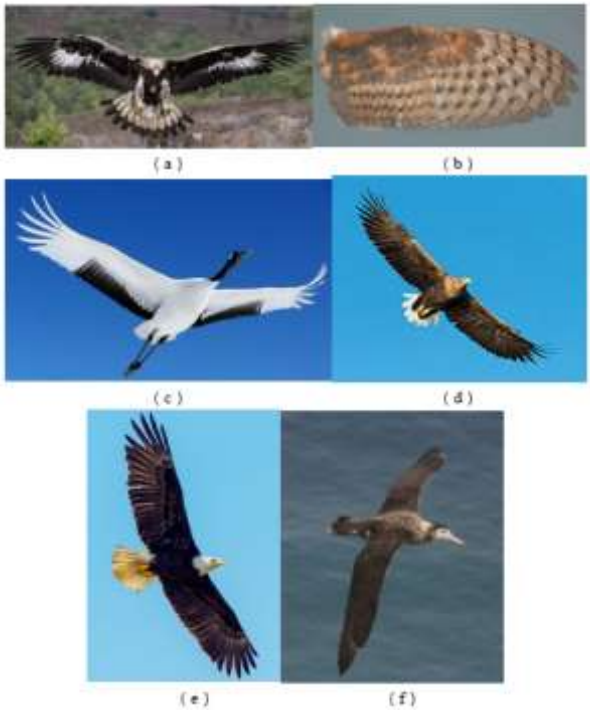

Figure 1 Flapping wings of some birds.

Referring to the above flapping wings and [20], a rectangular wing was taken as the research object to investigate the aerodynamic forces. A 3D model of the flapping wing is shown in Figure 2, from which it can be seen that the front end of the section is smooth while the back end is sharp. Such structures can both improve the wing's strength and produce strong aerodynamic forces.

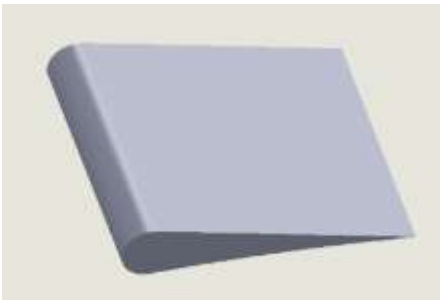

Figure 2 The physical model of the flapping wing.

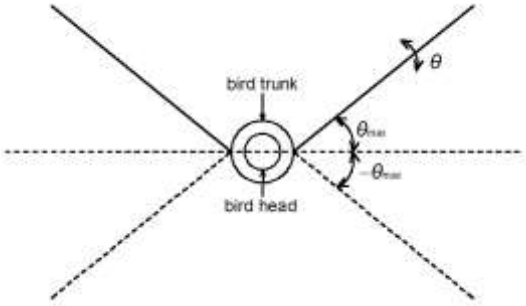

Figure 3 A schematic diagram of the robot's movement.

A bird-like robot can fly up and forward through the up-down flapping motion of its wings; a schematic diagram of this is shown in Figure 3. The aerodynamic forces are the same when the coordinates along the wingspan direction are the same. Based on the blade element theory, a tiny stripe is first selected to calculate its aerodynamic forces. Then, the tiny stripe is integrated along the full wingspan to obtain the aerodynamic forces over the entire flapping wing, which is shown in Figure 4. The wing usually flaps periodically and hence a cosine function is adopted to establish the kinematic model [21]. As presented in Figure 3, the flapping angle θ and its rate $\dot{\theta}(t)$ are expressed in Eqs. (1)-(2) respectively:

$$\theta(t) = \theta_{\max} \cos(2\pi f t) \tag{1}$$

$$\dot{\theta}(t) = -2\pi f \theta_{\max} \sin(2\pi f t) \tag{2}$$

where $\theta_{\max}$ is the maximum value of $\theta(t)$ and f is the flapping frequency.

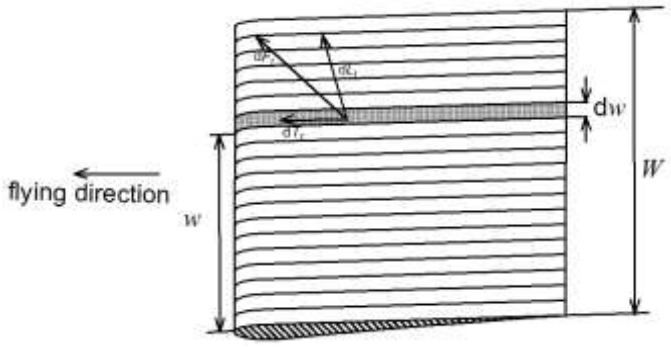

Figure 4 Flapping wing aerodynamic forces based on the blade element theory.

The pitching angle α can be expressed in Eq. (3) as follows:

$$\alpha(t) = \frac{w}{W}\alpha_{\max}\cos(2\pi ft + \varphi) \tag{3}$$

where w is the distance of the tiny stripe along the wingspan direction, W is half the length of the wingspan, $\alpha_{\max}$ is the maximum pitch angle, and φ is the lag angle between the pitching and flapping angles.

3 The Aerodynamic Model of the Bird-like Flapping Wing and its Influencing Parameters

In this section, the aerodynamic model of the bird-like flapping wing is established [21,22]. Then, the main influencing parameters of the aerodynamic forces are analyzed and multiple parameters are combined by the Taguchi orthogonal method.

3.1 The Aerodynamic Model

As shown in Figure 5, in order to analyze the forces of the bird-like flapping wing, three coordinate axes, namely, $X_f - Y_f$ (flapping axis), $X_w - Y_w$ (wind axis) and $X_b - Y_b$ (body axis) are established. In this case, the angle between $X_f - Y_f$ and $X_b - Y_b$ is α. The angle between $X_f - Y_f$ and $X_w - Y_w$ is γ. The angle between $X_b - Y_b$ and $X_w - Y_w$ is θ. When the robot flies along a forward horizontal direction, the aerodynamic forces on the flapping wing section include three parts: the section Joukowski lift ($\mathrm{d}N_1$), the section lift ($\mathrm{d}L_1$) and the section drag ($\mathrm{d}D$). These three forces are shown in Figure 5. The above forces are further analyzed below [21].

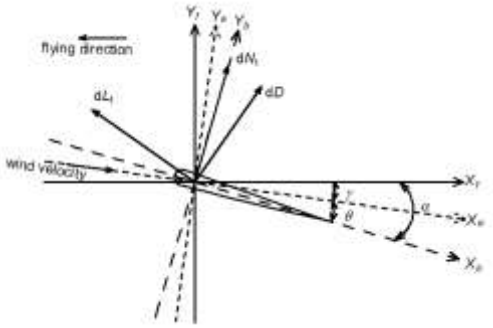

Figure 5 Three forces on the flapping wing section.

In Figure 6, the horizontal component v_x and the vertical component v_z of the relative wind velocity can respectively be represented in Eqs. (4) and (5) as follows:

$$v_x = v_f \cos\gamma + \left(0.75 c_h \dot{\alpha} \sin\alpha\right) \tag{4}$$

$$v_z = v_f \sin\gamma + \left(-w\dot{\theta}\cos\theta\right) + \left(0.75 c_h \dot{\alpha} \cos\theta\right) \tag{5}$$

where v_f is the flight velocity and c_h is the chord length.

On the wind axis ($X_w - Y_w$), the angle between v_x and v is ξ, and the relative incidence angle β can be expressed in Eq. (6) as:

$$v = \sqrt{v_x^2 + v_z^2};\ \xi = \tan^{-1}\left(\frac{v_z}{v_x}\right);\ \beta = \xi + \alpha \tag{6}$$

According to Figure 6, the angle between $\mathrm{d}D$ and v_x is equal to ξ, $\mathrm{d}D$ and $\mathrm{d}L_1$ are vertical to each other.

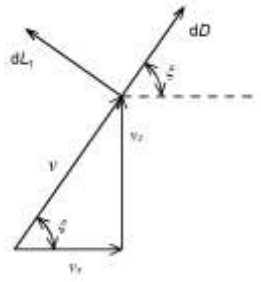

Figure 6 The relationship of some forces.

The section Joukowski lift $\mathrm{d}N_1$ is vertical to the wing surface and acts on the middle chord, which can be calculated according to the Kutta-Joukowski theorem in Eq. (7) as follows [22]:

$$\mathrm{d}N_1 = -\frac{\rho\pi c_h^2}{4}\left(\dot{\alpha} v_f + w\ddot{\theta}\cos\alpha - 0.5\ddot{\alpha}\right)\mathrm{d}w \tag{7}$$

where ρ is the air density.

The section lift $\mathrm{d}L_1$ can be calculated according to Eq. (8):

$$\mathrm{d}L_1 = \frac{1}{2}\rho v^2 c_1 c_h \mathrm{d}w \tag{8}$$

where the section lift coefficient $c_1 = 2\pi C(k)\sin\beta$, $C(k)$ is the Theodorsen function, c_h is the chord length, and dw is the tiny stripe width of the wing.

The section drag $\mathrm{d}D$ is expressed in Eq. (9) as follows:

$$\mathrm{d}D = \mathrm{d}D_1 + \mathrm{d}D_2 \tag{9}$$

where the profile drag $\mathrm{d}D_1$ and the induced drag $\mathrm{d}D_2$ can respectively be calculated by Eqs. (10)-(11):

$$\mathrm{d}D_1 = \frac{1}{2}\rho v^2 c_2 c_h \mathrm{d}w \tag{10}$$

$$\mathrm{d}D_2 = \frac{1}{2}\rho v^2 c_3 c_h \mathrm{d}w \tag{11}$$

where c_2 is the profile drag coefficient and c_3 is the induced drag coefficient.

The section Joukowski lift $\mathrm{d}N_1$, the section lift $\mathrm{d}L_1$ and the section drag $\mathrm{d}D$ are accordingly decomposed to obtain the tiny stripe lift $\mathrm{d}L_t$ and the tiny stripe thrust $\mathrm{d}T_t$, which are presented in Eqs. (12)-(13):

$$\mathrm{d}L_t = \mathrm{d}L_1\cos\xi\cos\gamma + \mathrm{d}N_1\cos(-\alpha)\cos\theta\cos\gamma + \mathrm{d}D\sin\xi\cos\gamma \tag{12}$$

$$\mathrm{d}T_t = \mathrm{d}L_1\sin\xi\cos\gamma + \mathrm{d}N_1\sin(-\alpha)\cos\theta\cos\gamma - \mathrm{d}D\cos\xi\cos\gamma \tag{13}$$

The tiny stripe lift $\mathrm{d}L_t$ and the tiny stripe thrust $\mathrm{d}T_t$ are integrated along the wingspan to obtain the lift $F_L(t)$ and the thrust $F_T(t)$ at a certain time, which is defined by Eq. (14):

$$\begin{cases} F_L(t) = \int_0^W \mathrm{d}L_t \\ F_T(t) = \int_0^W \mathrm{d}T_t \end{cases} \tag{14}$$

In order to evaluate the flapping wing performance from a comprehensive perspective, the lift $F_L(t)$ and the thrust $F_T(t)$ of the flapping wing are

integrated in a period T. The average lift $\overline{F}_L(t)$ and the average thrust $\overline{F}_T(t)$ can be expressed in Eq. (15) as follows:

$$\begin{cases} \overline{F}_L(t) = \dfrac{1}{T}\int_0^T F_L(t)\mathrm{d}t \\ \overline{F}_T(t) = \dfrac{1}{T}\int_0^T F_T(t)\mathrm{d}t \end{cases} \tag{15}$$

3.2 The Influencing Parameters of Aerodynamic Force

The lift and thrust can be adjusted by changing some important parameters to improve the robot's flying performance. However, it is tedious and time consuming to combine multiple parameters at multiple levels. In order to optimize the experimental numbers, the Taguchi orthogonal method was employed to study the aerodynamic force under multi-parameter combinations [23].

$L_9(3^4)$ is a Taguchi orthogonal array with 9 rows and 4 columns. As shown in Table 1, there are 4 parameters in the $L_9(3^4)$ orthogonal array, namely the flapping frequency, the maximum flapping angle, the flight velocity, and the incidence angle. Each parameter is featured with low, medium and high levels, which are respectively expressed by 1, 2 and 3. With the Taguchi orthogonal array mentioned above, the lift and thrust values under different combinations can be obtained using only 9 experiments.

Table 1 $L_9(3^4)$ Taguchi orthogonal array.

Experiment Number	Flapping frequency	Maximum flapping angle	Flight velocity	Incidence angle
1	1	1	1	1
2	1	2	2	2
3	1	3	3	3
4	2	1	2	3
5	2	2	3	1
6	2	3	1	2
7	3	1	3	2
8	3	2	1	3
9	3	3	2	1

4 Numerical Analysis

Referring to [24], a rectangular wing with a cross-sectional NACA0012 airfoil profile was taken as the research object, whose lift and thrust under different parameters were studied.

4.1 Aerodynamic Forces When a Parameter Changes

The flapping frequency, the maximum flapping angle, the flight velocity, and the incidence angle of the flapping wing were respectively set as $f = 10\text{Hz}$, $\theta_{\max} = 60°$, $v_f = 10\text{m/s}$ and $\gamma = 30°$. Then, the lift and the thrust dependent on time were calculated based on the aerodynamic model of the bird-like flapping wing from Section 3. The aerodynamic force curves in one flapping period are shown in Figure 7, which is similar to [25].

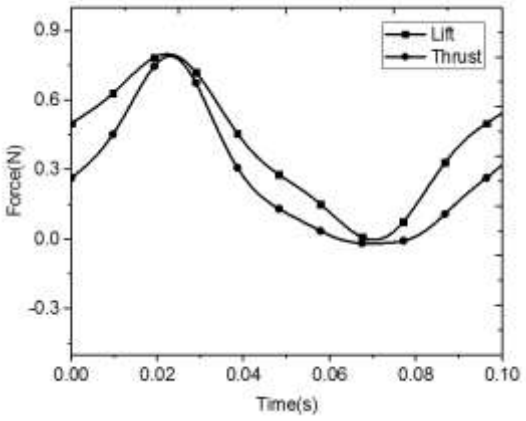

Figure 7 The aerodynamic force curves in one flapping period.

From Figure 7 it can be seen that the lift value is larger than the thrust value in one flapping period, which is consistent with [21] and [26]. By calculation, the average values of lift and thrust are 0.3997 and 0.2720. The large lift value can prevent the robot from falling down. The standard deviation values for lift and thrust are 0.2522 and 0.2567, which indicates that the dispersions of lift and thrust are similar.

In the following, the average lift and the average thrust defined in Eq. (15) are analyzed when some of the parameters change, as shown in Figure 8. It should be especially pointed out that Figures 8(a)-(d) were obtained by changing one parameter while keeping the other ones fixed. Similar to Figure 7, Figures 8(e)-(f) are the curves of aerodynamic force under different maximum flapping angles.

It can be seen from Figure 8(a) that both the value of $\overline{F}_L(t)$ and the value of $\overline{F}_T(t)$ are increased with the increase of the flapping frequency. Figure 8(b) clearly indicates that the flight velocity can increase the values of $\overline{F}_L(t)$ and

$\overline{F}_T(t)$. As shown in Figure 8(c), a parabolic shape appears when the values of $\overline{F}_L(t)$ and $\overline{F}_T(t)$ change with γ, therefore the aerodynamic forces are sensitive to the incidence angle. $\overline{F}_L(t)$ reaches a maximum value when $\gamma = 35°$, and $\overline{F}_T(t)$ reaches its maximum value when $\gamma = 55°$. It can also be seen that there is an obvious change between the first and second points of $\overline{F}_L(t)$; hence, the aerodynamic forces are especially sensitive to the incidence angle when its range is $0° - 5°$.

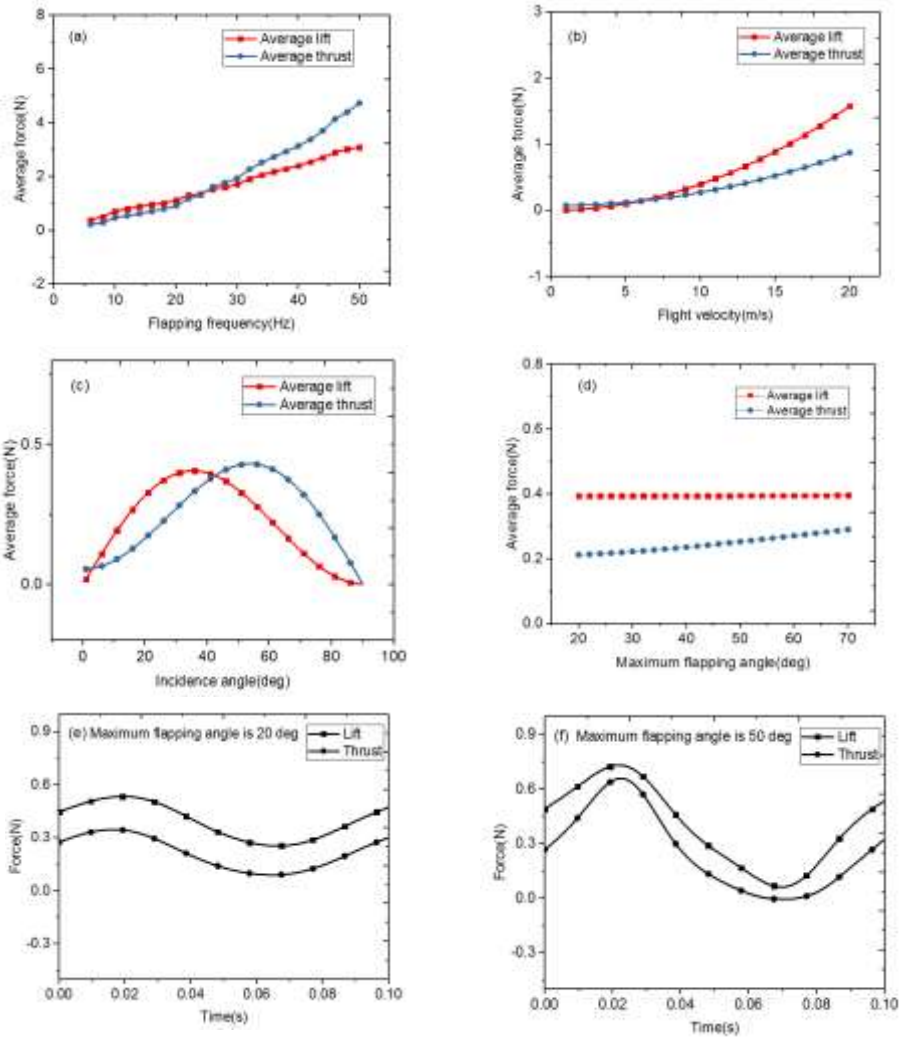

Figure 8 The curves of the aerodynamic force when some of the parameters change.

Figure 8(d) shows that the value of $\overline{F}_T(t)$ is slightly increased with the increase of the maximum flapping angle, while the value of $\overline{F}_L(t)$ is almost invariable, the trend of which is similar to [27]. Comparing Figure 8(e) with 8(f), it can be seen that the amplitudes of the lift are different, but the middle state is nearly the same. It is nearly symmetrical with the middle state and thus the values of $\overline{F}_L(t)$ with different the maximum flapping angle in Figure 8(d) are almost identical.

4.2 Aerodynamic Forces when Two or Three Parameters Change

In the following section, the values of $\overline{F}_L(t)$ and $\overline{F}_T(t)$ were calculated when two or three parameters changed. In Figure 9, the two horizontal axes are variable parameters and the vertical axis represents $\overline{F}_L(t)$, whose value is also represented by color.

According to Figure 9(a), the value of $\overline{F}_L(t)$ increases with the increase of the flapping frequency, while the maximum flapping angle has little effect on $\overline{F}_L(t)$. It is the flapping frequency rather than the flight velocity that can significantly increase the value of $\overline{F}_L(t)$, as shown in Figure 9(b). From Figure 9(c) it can be seen that the shape of $\overline{F}_L(t)$ is a paraboloid and $\overline{F}_L(t)$ has its maximum value when $\gamma = 35°$. Figure 9(d) shows that the flight velocity changes the value of $\overline{F}_L(t)$ more easily than the maximum flapping angle. Figure 9(e) indicates that the incidence angle is the main parameter that can be used to change the value of $\overline{F}_L(t)$ when the effect of the maximum flapping angle is weak. It can be seen from Figure 9(f) that the incidence angle cannot obviously cause a change of the value of $\overline{F}_L(t)$ if the flight velocity is lower than 10m/s. However, if the flight velocity is higher than 10m/s, then the value of $\overline{F}_L(t)$ can be easily changed by adjusting the incidence angle. Similar to Figure 9(b), $\overline{F}_L(t)$ increases with the increase of the flapping frequency in Figure 9(g). A tiny difference is that $\overline{F}_L(t)$ in Figure 9(g) is slightly larger than Figure 9(b) when both the flapping frequencies are high and the flight velocities are low.

According to Figures 10(a) and (b), the value of $\overline{F}_T(t)$ can be increased by increasing the flapping frequency. It can be seen from Figure 10(c) that the incidence angle has a slight effect on the value of $\overline{F}_T(t)$ when the flapping frequency is smaller than 20Hz. However, when the flapping frequency is higher than 20Hz, the value of $\overline{F}_T(t)$ becomes larger with the increase of the

incidence angle. From Figure 10(d) it can be obtained that $\overline{F}_T(t)$ is increased with the increase of the flight velocity. In Figure 10(e), the shape of $\overline{F}_T(t)$ appears as a paraboloid, which indicates that the incidence angle can increase the value of $\overline{F}_T(t)$ more easily than the maximum flapping angle.

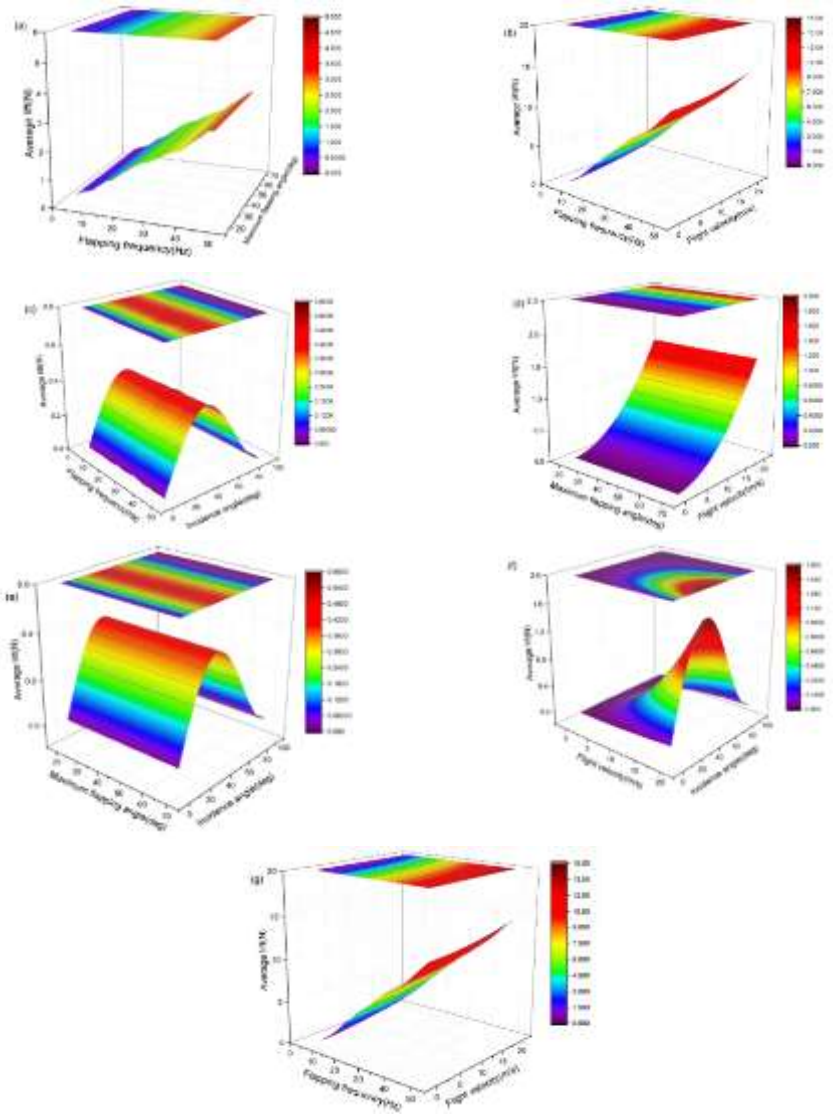

Figure 9 The values of $\overline{F}_L(t)$ for two variable parameters, where the incidence angle in (g) is set to $35°$.

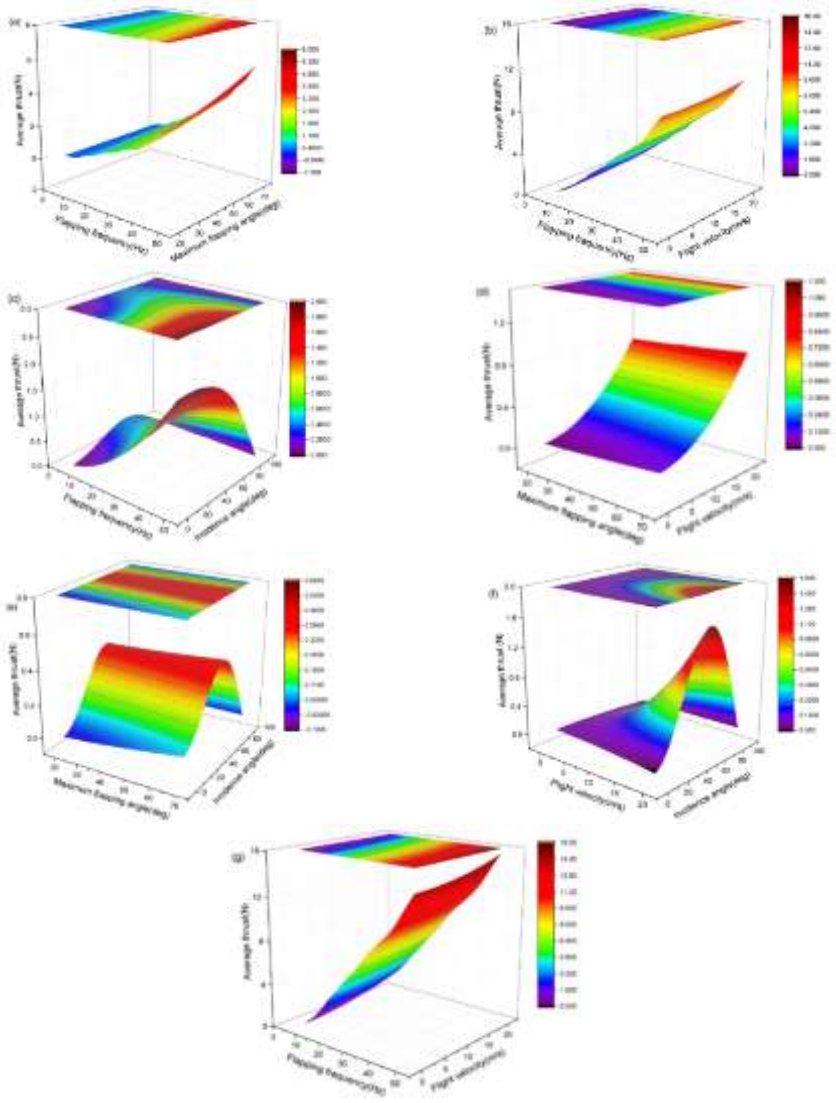

Figure 10 The values of $\overline{F}_T(t)$ for two variable parameters, where the incidence angle in (g) is set to $55°$.

Figure 10(f) shows the value of $\overline{F}_T(t)$ is easily influenced by the incidence angle and the flight velocity, $\overline{F}_T(t)$ reaches the maximum value when both $\gamma = 55°$ and the flight velocity is at the maximum value. From Figure 10(g),

$\overline{F}_T(t)$ increases with the increase of the flapping frequency. By comparing Figure 10(g) with (b) it can be seen that the average thrust with $55°$ incidence angle is obviously larger than the average thrust with $35°$ incidence angle. The reduced frequency $St = f \cdot c_h / v_f$ is an important parameter for flight efficiency. When the value of St is set to 0.25, the flight efficiency is usually high [28]. In other words, less energy will produce more useful aerodynamic forces. After confirming c_h, the reduced frequency St is mainly determined by both f and v_f. If there is one variable, the flight efficiency is high when $f = 44\text{Hz}$ or $v_f = 1.8\text{m/s}$. If there are two variables, many group parameters can let $St = 0.25$; which group is used is finally determined by experiment.

The following section discusses the average lift and average thrust of the bird-like flapping wing when three parameters were taken as variables.

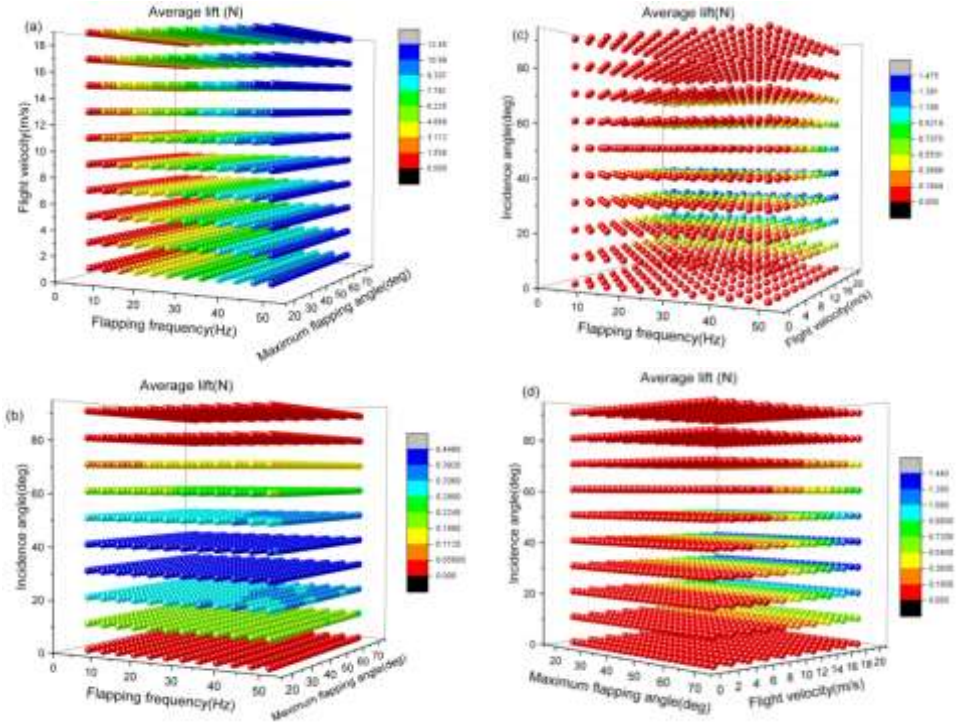

Figure 11 The values of $\overline{F}_L(t)$ for three variable parameters.

From Figure 11(a) it can be seen that the flapping frequency is the most important parameter that can be used to vary the value of $\overline{F}_L(t)$. According to Figure 11(b), compared with the maximum flapping angle and the flapping

frequency, the incidence angle can significantly affect the value of $\overline{F}_L(t)$. From Figure 11(c), the value of $\overline{F}_L(t)$ increases significantly with the increase of the flight velocity. According to Figure 11(d), when the incidence angle is within the range of $10°-70°$, the value of $\overline{F}_L(t)$ is sensitive to the flight velocity. Moreover, the maximum value of $\overline{F}_L(t)$ appears under the condition of a $30°-40°$ incidence angle and the highest flight velocity.

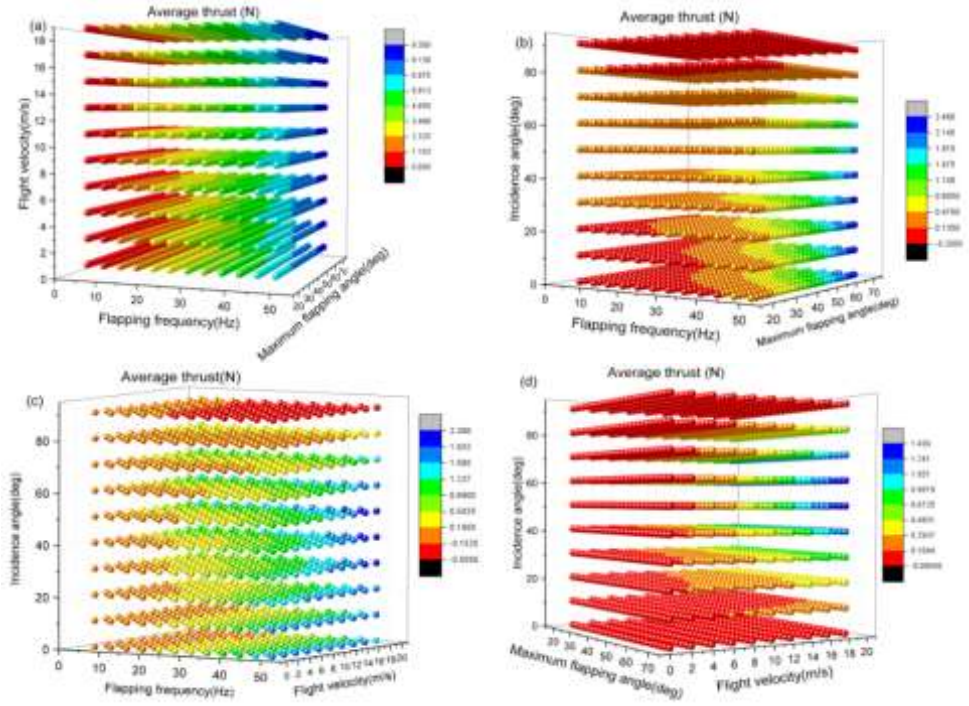

Figure 12 The values of $\overline{F}_T(t)$ for three variable parameters.

From Figure 12(a) it can be seen that the value of $\overline{F}_T(t)$ is significantly increased with the increase of flapping frequency. The maximum flapping angle can also to some extent cause a change in the value of $\overline{F}_T(t)$. The maximum value of $\overline{F}_T(t)$ appears when both the flapping frequency and the maximum flapping angle are at the maximum values. According to Figure 12(b), the maximum value of $\overline{F}_T(t)$ is obtained under the conditions where both the flapping frequency and the maximum flapping angle are at their maximum values and the incidence angle is in the range of $0°-50°$. From Figure 12(c), the value of $\overline{F}_T(t)$ becomes observably bigger with the increase of the flapping

frequency. According to Figure 12(d), $\overline{F}_T(t)$ reaches the maximum value when the interval of the incidence angle is $40°-60°$ and the flight velocity is the highest.

4.3 Aerodynamic Forces When All Parameters Change

The $L_9(3^4)$ Taguchi orthogonal array shown in Table 1 was adopted to study the values of $\overline{F}_L(t)$ and $\overline{F}_T(t)$. The parameters were separately set at three levels as follows: flapping frequencies $f_1 = 6\text{Hz}$, $f_2 = 28\text{Hz}$ and $f_3 = 50\text{Hz}$, maximum flapping angles $\theta_{\max 1} = 20$, $\theta_{\max 2} = 45$ and $\theta_{\max 3} = 70$, flight velocities $v_{f1} = 1\text{m/s}$, $v_{f2} = 10\text{m/s}$ and $v_{f3} = 20\text{m/s}$, and incidence angles $\gamma_1 = 1°$, $\gamma_2 = 20°$ and $\gamma_3 = 40°$. The histograms of $\overline{F}_L(t)$ and $\overline{F}_T(t)$ under different combinations are shown in Figure 13.

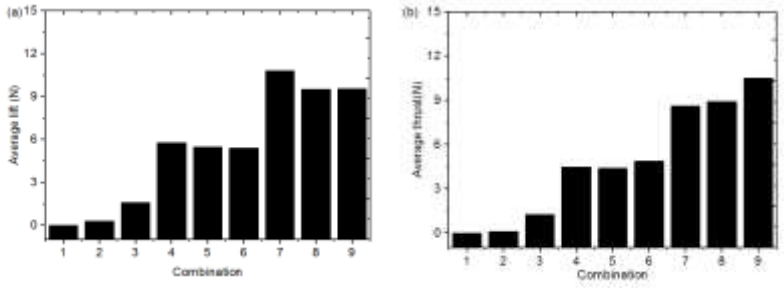

Figure 13 Histograms of $\overline{F}_L(t)$ and $\overline{F}_T(t)$ under different combinations.

According to Figure 13, the values of $\overline{F}_L(t)$ and $\overline{F}_T(t)$ can be divided into three groups: small values for combinations 1-3, medium values for combinations 4-6 and large values for combinations 7-9. The above differences mainly caused by the flapping frequencies in combinations 1-3, 4-6 and 7-9 are respectively set as level 1, level 2 and level 3. Therefore, the flapping frequency is the most important parameter affecting $\overline{F}_L(t)$ and $\overline{F}_T(t)$. Comparing combinations 7-9 in Figure 13(a), it can be seen that $\overline{F}_L(t)$ reaches the maximum value at combination 7. According to Table 1, the flight velocity in combination 7 is set as level 3. Therefore, the flight velocity has a notable impact on $\overline{F}_L(t)$. From combinations 7-9 in Figure 13(b) it can be seen that the maximum flapping angle can to some extent change $\overline{F}_T(t)$.

For an overall comparison of the simulation results, the results in Figures 8-13 were made uniform in Table 2. The symbols "○", "¤" and "●" respectively

represent parameters with weak, general and strong impacts on $\overline{F}_L(t)$ or $\overline{F}_T(t)$. The comprehensive index E is defined by Eq. (16) to evaluate the parameters' influences on $\overline{F}_L(t)$ or $\overline{F}_T(t)$:

$$E = \sum \Delta F \times c_s \tag{16}$$

where $\Delta F = F_{\max} - F_{\min}$, $F_{\max}$ and $F_{\min}$ are the maximum and minimum values of $\overline{F}_L(t)$ or $\overline{F}_T(t)$. c_s is the comprehensive index coefficient. For the symbols "○", "¤" and "●", c_s is separately set as $c_s = 0.01$, 0.05 and 0.1.

Table 2 Statistics of Parameter Impacts on $\overline{F}_L(t)$ or $\overline{F}_T(t)$ in Figures 8-13.

Parameters	$\overline{F}_L(t)$					$\overline{F}_T(t)$				
	ΔF	f	$\theta_{\max}$	v_f	γ	ΔF	f	$\theta_{\max}$	v_f	γ
One parameter	3.08	●				4.73	●			
	0		○			0.08		¤		
	1.58			●		0.8			●	
	0.41				●	0.43				●
Two parameters	2.84	●	○			5.27	●	¤		
	13.95	●		○		10.61	●		○	
	0.42	○			●	2.04	●			●
	1.57		○	●		0.88		○	●	
	0.41		○		●	0.46		¤		●
	1.62			●	●	1.6			●	●
Three parameters	12.43	●	○	¤		9.27	●	¤	¤	
	0.45	¤	¤		●	2.67	¤	●		¤
	1.47	○		●	●	2.77	●		¤	●
	1.44		○	●	●	1.51		¤	●	●
Four parameters	10.8	●	○	¤	○	10.5	●	¤	○	○
E		4.37	0.32	2.07	0.73		4.65	1.63	1.29	1.12

From Table 2, it can be clearly seen that increasing the flapping frequency is the most important way to enhance the value of $\overline{F}_L(t)$. $\overline{F}_L(t)$ can also be increased by the flight velocity. It has a weak effect on $\overline{F}_L(t)$ by changing the maximum flapping angle or the incidence angle. For $\overline{F}_T(t)$, the comprehensive indexes E values of the flapping frequency, the maximum flapping angle, the flight velocity and the incidence angle are 4.65, 1.63, 1.29 and 1.12 respectively. Therefore, the main measures used for enhancing the value of $\overline{F}_T(t)$ are increasing the flapping frequency and increasing the maximum flapping angle.

5 Conclusions

The aerodynamic forces of bird-like flapping wing robots mainly consist of lift and thrust, which should be adjusted in a timely manner according to a specific flying situation. Therefore, it is extremely important to study which parameters can effectively adjust the aerodynamic forces.

The sensitivity of the aerodynamic forces to multi-parameters in a bird-like flapping wing was studied in this work. First, the physical model and the kinematic model of the bird-like flapping wing were separately established. Second, the aerodynamic model of the flapping wing was built based on the blade element theory, the aerodynamic forces under multi-parameters were studied by adopting the Taguchi orthogonal method. The following conclusions were obtained from the numerical simulation. According to the influence on lift from strong to weak, the parameters can be ordered as follows: the flapping frequency, the flight velocity, the incidence angle and the maximum flapping angle. The parameter order according to their effect on thrust is: the flapping frequency, the maximum flapping angle, the flight velocity and the incidence angle. Increasing the flapping frequency is the most important method that can be used to enhance the lift and the thrust. The lift increases with the increase of the flight velocity, while the thrust can be enhanced by increasing the maximum flapping angle. The lift or the thrust attains maximum values within the conditions of a $35°$ or $55°$ incidence angle. The maximum values of lift or thrust appears when the effects of the above parameters on the lift or the thrust are the strongest.

In this work, some methods for adjusting the aerodynamic forces of a single-joint wing were obtained. As the structure's strength is extremely important to reach the aerodynamic forces, which will be studied in our future work.

Acknowledgement

This study was supported by the Scientific Research Project of Zhejiang Provincial Education Department in 2017 (No. Y201737651).

References

[1] Toshiyuki, N., Liu, H. & Bomphrey, R. J., *A CFD-informed Quasi-steady Model of Flapping Wing Aerodynamics*, Journal of Fluid Mechanics, **783**, pp. 323-343, 2015.

[2] Stewart, E., Patil, M., Canfield, R. & Snyder, R.D., *Parametric Representation and Shape Optimization of a Wing for Flapping Micro*

Air Vehicles, International Journal of Micro Air Vehicles, **4**(4), pp. 179-202, 2013.

[3] Phan, H.V., Truong, Q.T., Au, T.K. & Park, H.C., *Optimal Flapping Wing for Maximum Vertical Aerodynamic Force in Hover: Twisted or Flat*?, Bioinspiration & Biomimetics, **11**(4), pp. 046007, 2016.

[4] Sujoy, M. & Ranjan, G., *Nonlinear Dynamic Analysis of Dragonfly-inspired Piezoelectric Unimorph Actuated Flapping and Twisting Wing*, International Journal of Smart & Nano Materials**, 3**(2), pp. 103-122, 2012.

[5] Truong, Q.T., Nguyen, Q.V., Truong, V.T., Park, H.C., Byun, D.Y. & Goo, N.S., *Estimation of Force Generated by a Beetle-mimicking Flapping Wing System by Using the Blade Element Theory*, Proceedings of SPIE - The International Society for Optical Engineering, 79750M-79750M-11, 2011.

[6] Yang, Y. & Xie, Y.*, Aerodynamic Force Analysis on Wing of Bionic flapping wing Robot Based on Fluent*, Machine Tool & Hydraulics, **43**(15), pp. 163-165, 193, Aug. 2015.

[7] Yang, W.Q., Song, B.F., Song, W.P., Wang, L.G., Fu, P. & Xu, J.H., *Aerodynamic Research of Flexible Flapping Wing by Combining DIC and CFD Approaches*, 29th Congress of the International Council of the Aeronautical Sciences, pp. 1-7, Sep. 2014.

[8] Vinh, N.D., *Dynamics and Control of a Flapping Wing Aircraft*, Masters, Ho Chi Minh University of Technology, 2006.

[9] Zhang, X.J. & Hu, S.L., *Influence of Wing Shape on the Aerodynamic Characteristics of Flapping Wing Vehicle*, Flight Dynamics, **33**(1), pp. 18-20,25, Feb. 2015.

[10] Yang, W.Q., Song, B.F., Song, W.P. & Wang, L.G., *The Effects of Span-wise and Chord-wise Flexibility on the Aerodynamic Performance of Micro Flapping Wing*, Chinese Science Bulletin, **57**(22), pp. 2887-2897, 2012.

[11] Lua, K.B., Lim, T.T. & Yeo, K.S., *Effect of Wing–wake Interaction on Aerodynamic Force Generation on a 2D Flapping Wing*, Experiments in Fluids, **51**(1), pp. 177-195, 2011.

[12] Banerjee, A., Ghosh, S.K. & Das, D., *Aerodynamics of Flapping Wing at Low Reynolds Numbers: Force Measurement and Flow Visualization*, Isrn Mechanical Engineering, **2011**(23), 2014.

[13] Zhu, J. & Lei, B., *Effect of a Flapping Wing Geometry on its Aerodynamic Performance*, International Conference on Robotics and Automation Engineering, pp. 44-47, 2016.

[14] https://www.vcg.com/creative/809720339, retrieved 15 October, 2017.

[15] https://www.duitang.com/blog/?id=453389632, retrieved 15 October, 2017.

[16] http://www.photophoto.cn/show/14202187.html, retrieved 15 October, 2017.
[17] http://www.quanjing.com/imgbuy/ibxmcs04001411.html, retrieved 15 October, 2017.
[18] http://blog.sina.com.cn/s/blog_485b09aa0102vkca.html,15 October, 2017.
[19] https://baike.baidu.com/pic/%E4%BF%A1%E5%A4%A9%E7%BF%81/454705/21191299/6c63514a83a7c41009f7ef1c?fr=lemma&ct=cover#aid=207253&pic=11385343fbf2b211ae7e97bcca8065380dd78eeb, retrieved 15 October, 2017.
[20] Ou, K., Castonguay, P. & Jameson, A., *3D Flapping Wing Simulation with High Order Spectral Difference Method on Deformable Mesh*, 49th AIAA Aerospace Sciences Meeting, pp.1-17, Jan. 2011.
[21] Djojodihardjo, H., Ramli, A. S. S. & Wiriadidjaja, S., *Kinematic and Aerodynamic Modelling of Flapping Wing Ornithopter*, Procedia Engineering, **50**(9), pp. 848-863, 2012.
[22] Coclici, C.A. & Wendland, W.L., *On the Treatment of the Kutta-Joukowski Condition in Transonic Flow Computations*, Journal of Applied Mathematics and Mechanics, **79**(8), pp. 507-534, 2015.
[23] Taguchi, G., *Systems of Experimental Design: Engineering Methods to Optimize Quality and Minimize Costs*, UNIPUB⁄ Kraus International Publications, 1987.
[24] Durrani, N., Zaheer, S. & Qin, N., *Delaunay Graph Mapping-Based Mesh Deformation for Simulation of a Spanwise Rigid and Flexible Flapping NACA0012 Wing Using DES with Parallel Implementation*, Aiaa Aerospace Sciences Meeting Including the New Horizons Forum and Aerospace Exposition, pp. 1-14, 2011.
[25] Arabagi, V., Hines, L. & Sitti, M., *A Simulation and Design Tool for a Passive Rotation Flapping Wing Mechanism*, ASME Transactions on Mechatronics, **18**(2), pp. 787-798, 2013.
[26] Djojodihardjo, H. & Ramli, A. S. S., *Modeling Studies of Bi- and Quad-Wing Flapping Ornithopter Kinematics and Aerodynamics*, International Journal of Automotive & Mechanical Engineering, **9**, pp. 2180-1606, 2014.
[27] Yu, C.J. & Yan, H., *Aerodynamic Computation of Flapping-wing Simulating Pigeon*, Journal of Nanchang Hangkong University, **22**(2), pp. 39-43, 2008.
[28] Hu, Y.Q., *Some Dynamic Problems in Micro Air Vehicles*, Doctor Thesis of Nanjing University of Aeronautics and Astronautics, 2002.